Journal of Magnetism and Magnetic Materials 405 (2016) 66–71

Contents lists available at ScienceDirect

Journal of Magnetism and Magnetic Materials

journal homepage: www.elsevier.com/locate/jmmm

Current Perspectives

Phase composition, magnetic properties and thermal behavior of a novel Fe_2O_3–SiO_2 composite material

Alexander E. Panasenko [a,b,*], Ivan A. Tkachenko [a], Ludmila A. Zemnukhova [a,b], Igor V. Shchetinin [c], Nina A. Didenko [a]

[a] Institute of Chemistry, Far East Division, Russian Academy of Sciences, pr. Stoletiya Vladivostoka 159, 690022 Vladivostok, Russian Federation
[b] Far East Federal University, Sukhanova 8, 690950 Vladivostok, Russian Federation
[c] Moscow State Institute of Steel and Alloys (Technology University), Leninsky pr. 4, 117936 Moscow, Russian Federation

ARTICLE INFO

Article history:
Received 10 August 2015
Received in revised form
19 November 2015
Accepted 27 November 2015
Available online 18 December 2015

Keywords:
Composite materials
Nanoparticles
Magnetic properties
Iron oxides
Transition temperature

ABSTRACT

An Fe_2O_3–SiO_2 composite was prepared by controllable Fe^{3+} and SiO_3^{2-}hydrolysis. Scanning (SEM) and transmitting (TEM) electron microscopy images showed particles with an average size of 10–30 nm composed of an iron-containing core covered with a silica shell. The FT-IR, vibrating sample magnitometer (VSM), thermogravimetric analysis and Mössbauer spectroscopy study confirmed that the core consisted of ferrihydrite. Heating at 300 °C did not result in any noticeable phase transitions, whereas 800 °C heating caused the formation of the maghemite γ-Fe_2O_3 phase. Such improvement of the thermal stability of maghemite is promising for development of heat-resistant magnetic materials.

1. Introduction

Silica-based porous structured materials are of great interest for practical application as catalyst supports, sensing materials, adsorbents, and carriers for targeted drug delivery. The advantages are their ordered structure, highly specific surface, adjustable porosity and narrow pore size distribution.

Silica is widely used as a support material as its morphology and particle size can be easily controlled in comparison with other materials, and it has high thermal stability and mechanical strength. However, the separation of silica from a dispersion medium is inconvenient, which significantly narrows its application.

The combination of porous silica and magnetic nanoparticles is one way to produce new magnetic composite materials. Particles of this kind can be displaced by applying an external magnetic field, e.g. for the magnetic separation of a sorbent from a solution or for the targeted delivery of adsorbed drugs. Depending on the area of application of such materials, there are different requirements for their composition, morphology, adsorption and magnetic properties [1–5].

For optimal steerability of a composite material by an external magnetic field, its magnetization saturation (M_s) and magnetic susceptibility (χ) in weak fields have to be maximal. In contrast, remanence (M_r) and coercitivity (H_c) should be minimal to simplify dispergation and avoid the aggregation of particles. Low remanence assists in the aggregative stability of particles; from this perspective, magnetite Fe_3O_4 and maghemite γ-Fe_2O_3 have optimal magnetic properties among iron oxides. Besides, it is necessary to take into consideration that heat treatment of a magnetic material, for example, for regeneration of a sorbent, may change its magnetic properties, including irreversible phase transition.

Successful application of magnetic nanoparticles is highly dependent on the stability of the particles under a different external media. A nanoparticles are often chemically highly active due to high surface area, resulting generally in loss of magnetism. To chemically stabilize the magnetic nanoparticles they can be covered by protective silica layer. This kind of core–shell materials is attracting increasing attention [2,6,7].

Current methods for producing magnetic silica materials generally consist of the two-stage synthesis of a composition material from silicon dioxide and iron oxides. Such techniques imply the usage of organosilicon precursors, which is acceptable for laboratory synthesis, but significantly narrows their large-scale application in industry [8]. In this paper, we propose a new approach to a

* Corresponding author at: Institute of Chemistry, Far East Division, Russian Academy of Sciences, pr. Stoletiya Vladivostoka 159, 690022 Vladivostok, Russian Federation.
E-mail address: panasenko@ich.dvo.ru (A.E. Panasenko).

http://dx.doi.org/10.1016/j.jmmm.2015.11.087
0304-8853/

simple, cost efficient and environmentally safe synthesis of magnetic silica composite materials. The influence of synthesis conditions on structure, phase composition, and magnetic properties of the material have been investigated.

2. Experimental

2.1. Materials

Deionized water was used throughout this work. Iron chloride $FeCl_3 \cdot 6H_2O$ was chemical grade; all other chemicals, such as silica $SiO_2 \cdot nH_2O$, hydrochloric acid, sodium chloride, sodium hydroxide, ammonia (25% water solution) and acetone were of analytical grade and used as received.

2.2. Synthesis of magnetic composite materials

The composite materials Fe_2O_3–SiO_2 were prepared by two procedures. The first (I) consisted of the simultaneous hydrolysis of Fe^{3+} and SIO_3^{2-} ions followed by the formation of a co-precipitated non-structured composite material. For this purpose, $SiO_2 \cdot nH_2O$ was dissolved in 5 M NaOH, then the solution, under vigorous stirring, was slowly added to $FeCl_3 \cdot 6H_2O$ dissolved in 5% HCl at room temperature. Adding a relevant volume of HCl maintained the acidity at a predetermined constant level. The precipitate was centrifuged, washed with water and acetone and then air dried for 1 h at 105 °C (sp. I-1 – I-11 in Table 1).

The second procedure of composite synthesis (II) consisted of the deposition of silica layer on the colloid-size particles of iron hydroxide, forming a core–shell structure. Due to the addition of an excess of 25% ammonia solution to $FeCl_3 \cdot 6H_2O$ aqueous solution, a residue formed; this was filtered and washed with water. Hydrochloric acid was dropwise added into the water suspension of the fresh residue at 90 °C up to its full peptization. Then, the solution of SiO_2 in 5 M HCl was very slowly added at a temperature of 90 °C. The required amount of HCl was been added to maintain a constant pH = 9. After adding a predetermined amount of silica-containing solution, the acidity was adjusted to pH = 5 by HCl, and NaCl was added to an Na^+ concentration of 0.35 M. The reaction mixture was maintained at 90 °C for 1 h. The residue was filtered, rinsed with water and dried in air at 105 °C (sample II-105). Then, the material samples were annealed in a muffle furnace for 3 h at 300 and 800 °C (samples II-300 and II-800 correspondingly).

Table 1
Compositions of Fe_2O_3–SiO_2 composite materials depending on the synthesis conditions.

Synthesis procedures	Sample	Initial molar ratio Si: Fe	pH	Content, %	
				Fe_2O_3	H_2O
procedure I (drying at 105 °C)	I-1	1:0.1	1.3	13.9	22.8
	I-2	1:0.1	1.5	14.3	22.0
	I-3	1:0.1	1.6	18.6	21.8
	I-4	1:0.1	1.7	23.9	24.0
	I-5	1:0.1	1.8	29.8	20.2
	I-6	1:0.1	1.9	34.4	25.4
	I-7	1:0.1	2.2	34.2	24.6
	I-8	1:0.1	2.6	34.1	22.0
	I-9	1:0.25	2.6	36.3	18.0
	I-10	1:0.5	2.6	45.4	26.4
	I-11	1:1	2.6	63.9	11.8
procedure II	II-105	1:0.3	9.0	25.7	11.6
	II-300	1:0.3	9.0	26.8	9.0
	II-800	1:0.3	9.0	29.3	2.7

2.3. Characterization

The content of iron in the samples was determined by titration with Trilon B. Water content was determined gravimetrically after calcination at 1000 °C for 3 h. IR spectra were recorded on a Shimadzu FTIR Prestige-21 spectrophotometer at frequency range 4000–400 cm^{-1} and samples were measured in Vaseline mull. XRD measurements were performed on a Bruker D8 ADVANCE diffractometer, using Cu K_α radiation. The thermal analysis was done using a MOM Q-1000 derivatograph, heating rate of 5 K/min, the samples masses were 250 mg and 110 mg (samples I-3 and II-105 correspondingly), alumina calcinated up to 1000 °C was used as a reference. The particle size and morphology of the materials were observed by LEO EVO-50 XPV scanning electron microscope and Zeiss Libra 120 transmission electron microscope, respectively. The magnetic measurement was examined by Quantum Design PPMS 9 T ECII vibrating sample magnitometer (VSM) at temperatures of $2-300$ K and fields up to ± 5 T. Magnetic susceptibility χ was calculated in a weak field. The Mössbauer study was carried out by MOS-TEC MS1101E instrument, at room temperature. The γ-ray source is the isotope Co^{57}. The Mössbauer spectra are calibrated by means of a spectrum for a standard α-Fe sample.

3. Results and discussion

The co-precipitated (procedure I) composite materials are fine reddish-brown powders. Chemical analysis shows (Table 1) that iron content, calculated as Fe_2O_3, increased from 13.9% to 34.4% with an increase in pH from 1.3 to 1.9 (at initial molar ratio Si: Fe = 1:0.1). Further pH increase did not lead to growth of the iron content. Composite materials with an iron content up to 63.9% were obtained by varying the ratio of the initial reagents.

Procedure II was based on fact that SIO_4^{2-} anion hydrolysis in acidic media leads to gel formation, and also in basic media, to form polysilicic acid, directly from SiO_2 sole, so-called “active silica”. The deposition of silica in basic media is some slower, but allows a desired morphology to be obtained, e.g. silica coatings on particles of another substance [9]. The iron content in the as-synthesized composite material was 25.7% (sample II-105).

In co-precipitated composite material (sample I-4) according to SEM data particles size is about 100–150 nm. Isometric particles without any faceting forms aggregates that are 3 to 5 μm in size. Fig. 1 shows the SEM and TEM images of the composite material, obtained as per procedure II (sample II-105), which are composed of isometric particles with a size of ca. 10–30 nm, without faceting. From the TEM image (Fig. 1b), it can be seen that particles consist of a dark core (iron oxide), covered with a lighter shell (silica).

All of the synthesized composite materials are amorphous; the diffractograms (Fig. 2) exhibit two broad peaks at about $2\theta = 35°$ and 63°, typical of poorly crystalline iron oxides (ferrihydrite, maghemite and hematite) with crystals smaller than 3 nm [10,11]. In the case of iron content lower than 36.3% (samples I-1 – I-9) an additional peak appears at $2\theta \approx 24°$, which is typical for amorphous SiO_2 [5]. For the nanosized particles, XRD-based identification of a particular iron oxide is difficult because of significant peak broadening due to the size effect.

It is well known that the hydrolysis of acidic solutions of iron salts can result in various iron oxides and oxohydroxides, depending on the initial compounds and reaction conditions. The fast hydrolysis of Fe^{3+} solutions typically produces an amorphous non-stoichiometric hydrated oxohydroxide $Fe_2O_3 \cdot nH_2O$, which is also known as ferrihydrite. Its crystallinity, i.e. crystal size and ordering, is mostly lower than in any other iron oxide compounds. For poorly crystalline ferrihydrite, the presence of two broad peaks

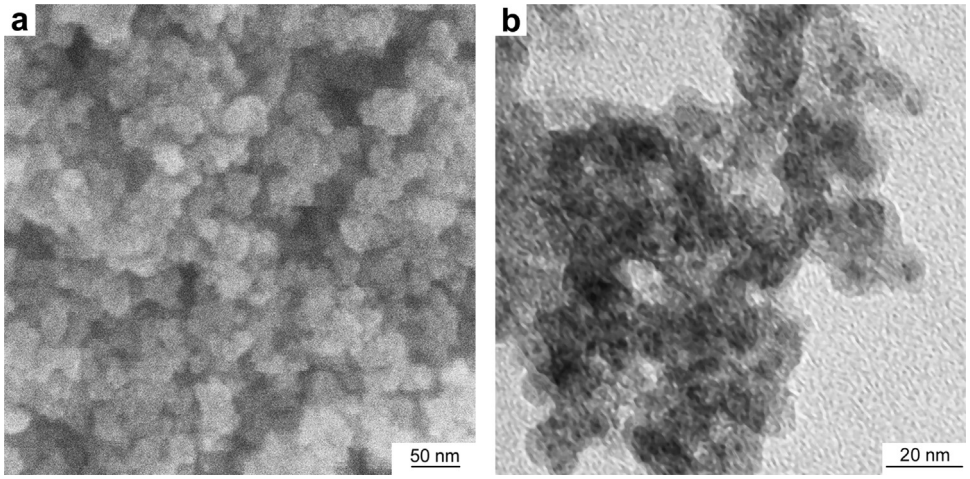

Fig. 1. SEM (a) and TEM (b) images of the composite Fe_2O_3–SiO_2 (sample II-105).

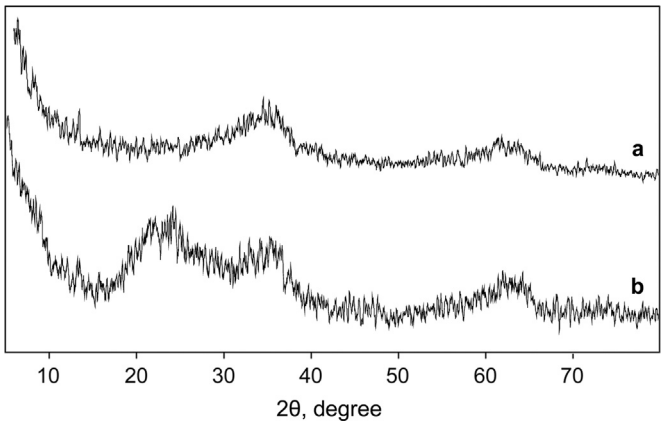

Fig. 2. XRD patterns of the composite materials (a) I-11 and (b) II-105 samples.

is typical on X-ray diffractograms [10], similar to Fig. 2a.

In view of iron-based composite materials being anticipated to be used as magnetoactive sorbents, materials with high magnetic susceptibility and saturation magnetization are of main interest. One such substance is maghemite, γ-Fe_2O_3, with high saturation magnetization. Maghemite is metastable, offers ferrimagnetic, ferromagnetic or superparamagnetic (for particles less than 10 nm) properties, and it can be obtained due to ferrihydrite thermal decomposition at 120–280 °C [6,12,13].

Upon further heating, maghemite transforms to hematite α-Fe_2O_3. The temperature of the transformation depends on particle size, water content, stoichiometry, and the presence of a foreign phase (in composition materials) or a foreign ion, such as Mg^{2+} and Fe^{2+}, and amounts 300 to 450 °C [10,14–19]. Hematite exhibits weak ferromagnetic properties, and it is an antiferromagnetic at temperatures lower than ~260 K (Morin transition temperature) [20].

The thermal properties of the two composite materials obtained by different procedures have been investigated by thermogravimetric and differential thermal analysis at temperature 25 to 800 °C. In DTA curves (Fig. 3), there are endothermic peaks at 120–160 °C which are attributed to the evaporation of physically absorbed water. The weight loss occurring at 200 °C was 16.0% and 4.5% for samples I-3 and II-105, respectively. The DTA curves show exothermic peaks at 200–360 °C that are related to the recrystallization of smaller crystals into larger ones [10]. Depending on the synthesis conditions of composite materials, the position and intensity of exothermic peaks are varying. Composite II-105 has broader peaks at higher temperatures, which are probably correlated with the encapsulation of iron oxides in the core–shell structure. Generally, the thermal behavior of the samples in the range of 200–360 °C is similar to that of ferrihydrite. Heating to over 360 °C leads to a gradual weight loss, which is related to removal of chemically bonded water. Total weight loss at 800 °C reaches 22.4% and 9.1% for I-3 and II-105 samples, respectively.

Differences in the chemical composition of the composite materials after heating at 105, 300 and 800 °C are shown in Table 1 (samples II-105, II-300, and II-800). After thermal treatment on XRD patterns, all of the peaks remain broad and no new reflexes appear, enabling the phase composition of iron oxides to be identified.

FT-IR spectra of composite Fe_2O_3–SiO_2 materials are less informative for the identification of iron oxides as well, because silica spectrum has the strong band about 470 cm^{-1} and a number of medium bands at 546, 800 and 964 cm^{-1}, which overlap with characteristic absorption peaks of the Fe–O bond. As such, the FT-IR spectrum of the as-prepared composite material is nearly identical to those of precipitated silica (Fig. 4a). However, after heating of the composite material at 800 °C, an absorption peak at 570–590 $см^{-1}$ (Fig. 4c) appears in the spectrum. The position of the peak allows it to be related to the Fe–O vibrations in maghemite γ-Fe_2O_3. In addition, the band at 540 cm^{-1}, which is characteristic for hematite α-Fe_2O_3, did not appear.

Figs. 5 and 6 shows the magnetization curves and the temperature dependence of the magnetization curves registered under zero field cooling (ZFC) and field cooling in 200 Oe field (FC) for the two types of composite materials in comparison with maghemite γ-Fe_2O_3. A common feature of all samples is a misalignment of FC and ZFC curves and an increase of the magnetization curve slope at low temperatures. The difference between FC and ZFC curves gives evidence of the superparamagnetic character of an ensemble of particles in the samples. As is already known, in the absence of magnetic field, magnetic moments of superparamagnetic particles are oriented randomly, resulting in zero total magnetic moment. Cooling in the absence of magnetic field leads to “freezing” of magnetic moments at a magnetic blocking temperature, T_b, while moment orientation remains chaotic, and total magnetic moment still remain zero. T_b depends on particle volume and anisotropy (in case of constant anisotropy, only on volume). The greater the particle volume, the higher the blocking temperature:

$$T_b = KV/25k_B, \quad (1)$$

where K is the anisotropy constant, V the volume, and k_B the Boltzmann constant. On cooling in the magnetic field, magnetic

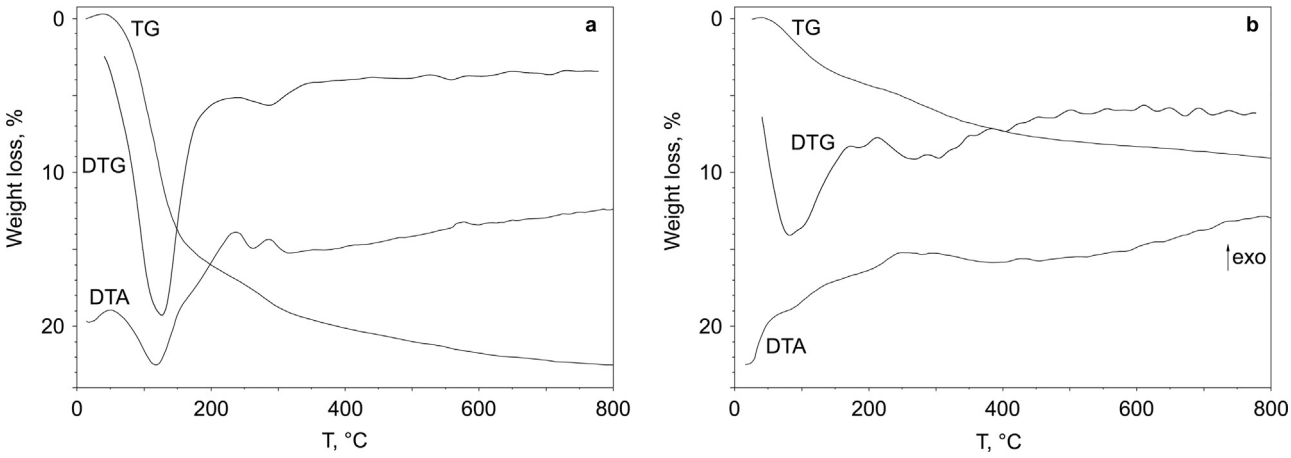

Fig. 3. Thermogravimetric analysis (TG and DTG) and differential thermal analysis (DTA) curves of (a) I-3 and (b) II-105 composite materials.

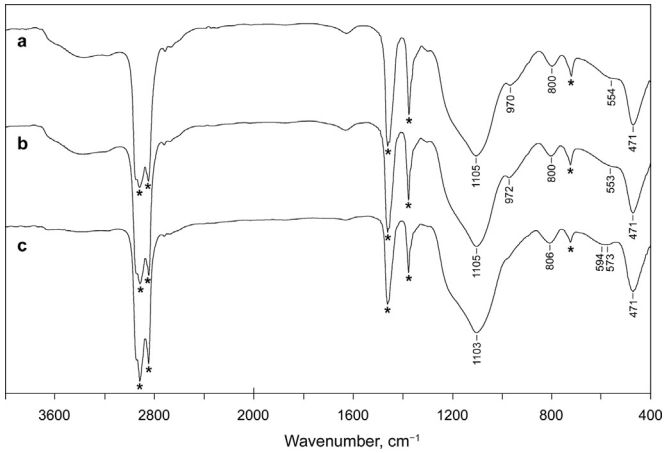

Fig. 4. FT-IR spectra of (a) II-105, (b) II-300, and (c) II-800 samples (asterisk marks Vaseline absorption bands).

moments of particles align along the applied field, and after blocking, the sample is magnetized to saturation (M_s).

In a real sample, some particle size distribution exists and a blocking temperature distribution follows on from this. Total magnetization increases gradually with increasing temperature, and the ZFC curve has a fairly wide peak. At temperatures higher than T_b, the magnetization begins to relax and decreases with increasing temperature. Therefore, the real peak on a ZFC curve is a superposition of narrow peaks, corresponding to various size particles, and the maximal contribution denotes particles constituting a major volume. Fig. 6 shows a significant difference between FC and ZFC curves for all of the samples investigated.

Sample I-9 exhibited the narrowest peak on a ZFC curve and the lowest $T_b \approx 6$ K (Fig. 6a, Table 2). Based on Eq. (1), as well as assuming that magnetic anisotropy constant for all the samples investigated is the same, we concluded that sample I-9 has the lowest size magnetic particles of the samples I-9 – I-11 – II-105. Another sample has peaks on ZFC curves at higher temperatures: sample I-11 at ~24 K and sample II-105 at ~20 K.

Magnetization curves (Fig. 5d) show that sample II-300 has the highest coercitivity, which probably indicates that core–shell composites (procedure II) include nanosized magnetic particles more related to a single-domain structure than particles in co-precipitated composites (samples I-9 and I-11). It should be noted, as well, that for samples II-105 and II-300 at 3 K, the magnetic hysteresis loop is shifted to a negative field. It is known that this shift can be espied in a large variety of systems which are composed by an antiferromagnet that is in atomic contact with a ferromagnet [21,22]. The shift of the center of magnetic hysteresis loop from its normal position at H=0 to H≠0, known as exchange anisotropy, occurs after the system is cooled in an external field. The phenomenon is considered to be associated with an intreface exchange interaction between ferromagnet and antiferromagnet magnetic moments. For the samples investigated magnetization curves were recorded after cooling the samples in the external field. Taking the above-mentioned into account, we can conclude that the shift of hysteresis loop to a negative field indicates the presence of ferromagnetic–antiferromagnetic exchange, which can significantly increase coercitivity as well [21,22].

Figs. 5b, d and 6b show the field and temperature dependence of the magnetization curves for the samples heated at different temperatures. Magnetic properties of the samples heated at 105 °C and 300 °C are nearly identical. Heating at 800 °C results in normalized magnetization (unit-mass Fe_2O_3) rapidly increasing. In addition, blocking temperature increases from 18 to 28 K and misalignment of T_b and point of no return appears, that not observed for any other samples. The resulting T_b is similar to literature data for the nanocomposite γ-Fe_2O_3/SiO_2 with particles of 4–5 nm [23]. It is worthwhile noting that commonly heating iron oxide at 800 °C leads to the formation of a low magnetic hematite phase. In the case of composite material, magnetization increases. It appears that the silica shell prevents maghemite–hematite phase transition.

In particular, it should be pointed out that fine-grained maghemite γ-Fe_2O_3 obtained by the fast hydrolysis of $FeCl_3$ with subsequent precipitate washing, drying and heating, is a superparamagnetic with a blocking temperature of about 75 K (Fig. 6b), in contrast to ferrimagnetic bulk maghemite [10]. However, the curvature of FC line and feature of magnetization curves registered at 300 and 3 K shows that a magnetic transformation near T_b exists, which requires additional investigation to refine its nature.

3.1. Mössbauer spectroscopy

Among the spectroscopic methods, Mössbauer spectroscopy (nuclear resonant γ-ray absorption spectroscopy) has the great advantage of being element-specific and, as ^{57}Fe is a convenient Mössbauer active isotope, the technique is suitable for iron oxides. It supplies information about the magnetic field at the nucleus, the valence of the Fe and the type of coordination and order within the ligand shell.

As is known, the Mössbauer isomer shift, δ, depends on the electron wave function and is different in different nuclear physical or chemical environments, so it can provide information about element oxidation state. Quadrupole splitting, ε, in the

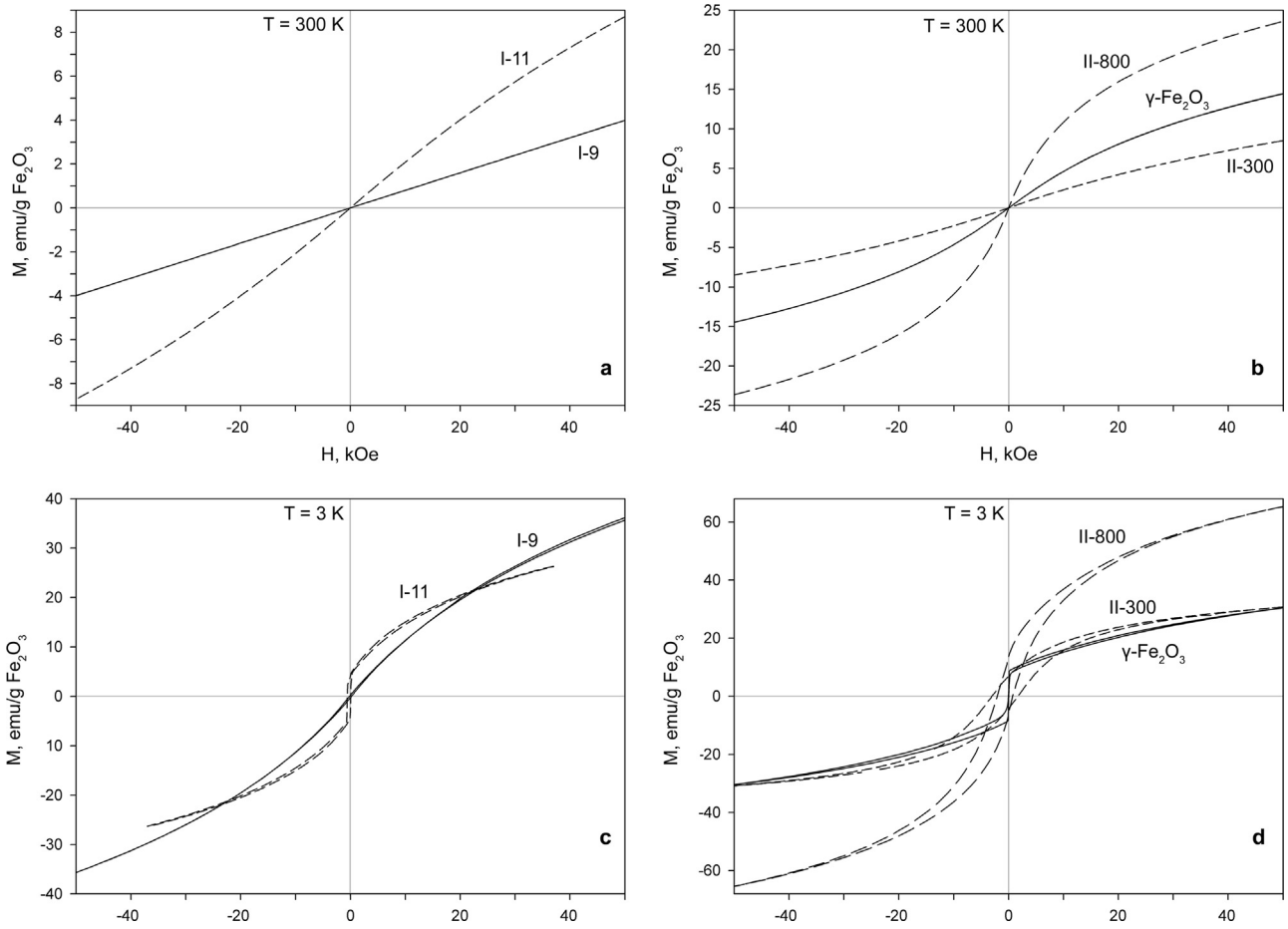

Fig. 5. Magnetization curves of composite materials Fe_2O_3–SiO_2 and γ-Fe_2O_3 registered at (a, b) 300 K and (c, d) 3 K.

Mössbauer spectrum responds to a quadrupole interaction between the nucleus and external electric field gradient. Its value provides information about nucleus coordination symmetry and a number of nonequivalent atomic positions [10,23].

The Mössbauer spectra of the II-105 and II-300 samples are doublets with similar parameters (Table 3) in agreement with ferric ion (Fe^{3+}) on a paramagnetic or superparamagnetic site. At room temperature, exhibiting only a doublet in Mössbauer spectrum is typical for a nanometer-sized poorly crystalline maghemite and hematite as well as ferrihydrite, irrespective of crystallinity; for all of them, Mössbauer parameters are relatively equal [11,24].

After heating the composite material at 800 °C (sample II-800), its spectrum can be fitted with two superpositioned doublets, the first with parameters close to the doublets in II-105 and II-300 sample spectra, and the second doublet with a significantly higher $\varepsilon = 1.10$ (Table 3). As quadrupole splitting is positively related to an electric field gradient near the nucleus, it appears that heating results in a reduction of symmetry of the nuclear charge environment. The most probable cause is the formation of units of a crystal structure with not only octahedral, but also tetrahedral Fe sites. This appears to be maghemite γ-Fe_2O_3, with a spinel structure with two sublattices. The isomer shifts of 0.31 and 0.34 mm/s

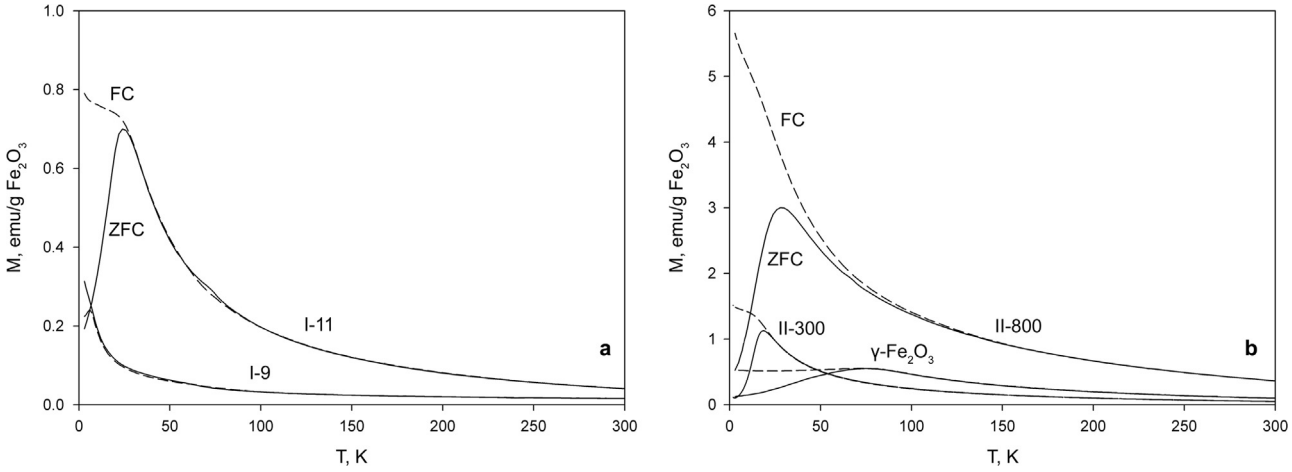

Fig. 6. Temperature dependence of the magnetization curves under ZFC and FC for the Fe_2O_3–SiO_2 composite materials and γ-Fe_2O_3 at field of 200 Oe.

Table 2
Magnetic parameters for the Fe_2O_3–SiO_2 composites and iron oxides.

Sample	M_r, emu/g	χ	T_b, K
I-9	$3.58 \cdot 10^{-4}$	$3.27 \cdot 10^{-5}$	6.0
I-11	$1.62 \cdot 10^{-3}$	$1.50 \cdot 10^{-4}$	24
II-105	$3.20 \cdot 10^{-3}$	$5.02 \cdot 10^{-5}$	18
II-300	$4.03 \cdot 10^{-3}$	$6.10 \cdot 10^{-5}$	20
II-800	$4.73 \cdot 10^{-3}$	$5.43 \cdot 10^{-4}$	28
ferrihydrite	$2.11 \cdot 10^{-3}$	$3.47 \cdot 10^{-4}$	ND
γ-Fe_2O_3	$7.58 \cdot 10^{-3}$	$4.90 \cdot 10^{-4}$	76
α-Fe_2O_3	0.167	$7.32 \cdot 10^{-5}$	–

Table 3
Mössbauer parameters for the Fe_2O_3–SiO_2 composites.

Sample	δ, mm/s	ε, mm/s	Reference
II-105	0.34	0.68	
II-300	0.35	0.72	
II-800 Doublet 1 (73.16%)	0.34	0.65	
II-800 Doublet 2 (26.84%)	0.31	1.10	
ferrihydrite	0.35	0.62	[6,24]
	0.35	0.78	
γ-Fe_2O_3	0.35	≤ 0.02	[6,23]
γ-Fe_2O_3 (nanoparticles)	0.32–0.35	0.75–0.90	[23]
α-Fe_2O_3	0.37–0.39	0.02–0.09	[25]
α-Fe_2O_3 (nanoparticles)	0.30–0.35	0.66–0.78	[11,25]

are in good agreement with the isomer shifts reported for γ-Fe_2O_3 [6,23]. In addition, significant increasing of magnetization of II-800 sample relative to II-300 favouring just maghemite formation, as well as thermal analysis and FT-IR spectroscopy data.

Well-crystallized maghemite in the Mössbauer spectrum exhibits a sextet resulting from Zeeman splitting, occurring in a magnetic field, which is typical for magnetically ordered materials [10]. In the material investigated (sample II-800), due to its fine dispersity, the magnetic order is low and internal field is near-zero ($M_r = 4.73 \cdot 10^{-3}$ emu/g); thus, the splitting of spectral lines does not occur.

Opening the question of iron oxides phase identification, it is should be said that the decrease in particle size gradually eliminates distinctions in individual features of iron oxides and certainly differ from bulk substances [13].

4. Conclusions

In summary, a simple and inexpensive Fe_2O_3–SiO_2 composite material was synthesized. Sets of X-ray diffraction, thermogravimetric analysis, vibrating sample magnitometry, FT-IR and Mössbauer spectroscopy data proved that in the composite material heated to 105 °C, iron was in the form of ferrihydrite without a long-range ordered crystal structure. In contrast with a bulk ferrihydrite, commonly decomposing at 120–150 °C, the core–shell structured composites heated at 300 °C did not suffer phase transitions. Further heating of the composite at 800 °C resulted in maghemite formation with no evidence of hematite, whereas maghemite alone commonly transforms to a hematite even at 400–600 °C. Such augmentation of the thermal stability of ferrihydrite and maghemite into the silica matrix is attributable to an influence of composite material structure, which curbs nanoparticles growth and, as a consequence, prevents phase transformation.

Acknowledgments

The authors thank N.N. Barinov (Laboratory of Micro- and Nanoscale Researches, Far East Geological Institute FEB RAS), and D.V. Fomin (Laboratory of Electron Microscopy, Institute of Marine Biology FEB RAS) for their assistance in the TEM studies.

References

[1] Y. Deng, Y. Cai, Z. Sun, D. Zhao, Chem. Phys. Lett. 510 (2011) 1.
[2] P. Zong, S. Wang, Y. Zhao, H. Wang, H. Pan, C. He, Chem. Eng. J. 220 (2013) 45.
[3] Z. Jia, K. Peng, Y. Li, R. Zhu, Mat. Sci. Eng. B 176 (2011) 861.
[4] H.Y. Zhu, R. Jiang, Y.-Q. Fu, J.-H. Jiang, L. Xiao, G.-M. Zeng, Appl. Surf. Sci. 258 (2011) 1337.
[5] J. Zhao, Y. Wang, G. Luo, S. Zhu, Particuology 9 (2011) 56.
[6] E. Murad, Phys. Chem. Min. 23 (1996) 248.
[7] M. Mahmoudi, S. Sant, B. Wang, S. Laurent, T. Sen, Adv. Drug. Deliv. Rev. 63 (2011) 24.
[8] S. Sadeghi, H. Azhdaria, H. Arabib, A.Z. Moghaddama, J. Hazard. Mater. 215–216 (2012) 208.
[9] R.K. Iler, The Chemistry of Silica: Solubility, Polymerization, Colloid and Surface Properties and Biochemistry of Silica, A Wiley-Interscience Publication, New York–Chichester–Brisbano–Toronto, 1979.
[10] U. Schwertmann, R.M. Cornell, Iron Oxides in the Laboratory, Second Edition, Wiley-VCH, Weinheim, 2000.
[11] R.V. Morris, D.C. Golden, J.F. Bell III, H.V. Lauer Jr, J.B. Adams, Geochim. Cosmochim. Acta 57 (1993) 4597.
[12] C.E. Housecroft, A.G. Sharpe, Inorganic Chemistry, 3rd Edition, Pearson, London, United Kingdom, 2008.
[13] H. Stanjek, P.G. Weidler, Clay Miner. 27 (1992) 397.
[14] C.M. Keefer, P.N. Shive, Earth Planet. Sci. Lett. 51 (1980) 199.
[15] C.M. Keefer, P.N. Shive, J. Geophys. Res. 86 (1981) 987.
[16] D.J. Dunlop, O. Ozdemir, Rock Magnetism: Fundamentals and Frontiers, Cambridge Univ. Press, Cambridge, United Kingdom, 1997.
[17] T.S. Gendler, V.P. Shcherbakov, M.J. Dekkers, A.K. Gapeev, S.K. Gribov, E. Mc Clelland, Geophys. J. Int. 160 (2005) 815.
[18] O. Ozdemir, S.K. Banerjee, Geophys. Res. Lett. 11 (1984) 161.
[19] O. Ozdemir, Phys. Earth Planet. Inter. 65 (1990) 125.
[20] J.E. Greedon, Magnetic oxides, Encyclopedia of Inorganic chemistry, New York, 1994.
[21] J. Nogues, I.K. Schuller, J. Magn. Magn. Mater. 192 (1999) 203.
[22] M. Kiwi M, J. Magn. Magn. Mater. 234 (2001) 584.
[23] L. Zhang, G.C. Papaefthymiou, J.Y. Ying, J. Appl. Phys. 81 (1997) 6892.
[24] E. Murad, U. Schwertmann, Am. Miner. 65 (1980) 1044.
[25] M.I. Ivanovskaya, D.A. Kotsikau, A. Taurino, P. Siciliano, Sens. Actuators B 124 (2007) 133.